2018

Electronic structure of electron-irradiated graphene and effects of hydrogen passivation

Asanka Weerasinghe
University of Massachusetts Amherst

Ashwin Ramasubramaniam
University of Massachusetts Amherst

Dimitrios Maroudas
University of Massachusetts Amherst

Recommended Citation
Weerasinghe, Asanka; Ramasubramaniam, Ashwin; and Maroudas, Dimitrios, "Electronic structure of electron-irradiated graphene and effects of hydrogen passivation" (2018). *Materials Research Express*. 619.
https://doi.org/10.1088/2053-1591/aaddce

Materials Research Express

PAPER

Electronic structure of electron-irradiated graphene and effects of hydrogen passivation

Materials Research Express

PAPER

Electronic structure of electron-irradiated graphene and effects of hydrogen passivation

RECEIVED
9 August 2018

REVISED
22 August 2018

ACCEPTED FOR PUBLICATION
30 August 2018

PUBLISHED
12 September 2018

Asanka Weerasinghe[1], **Ashwin Ramasubramaniam**[2] **and Dimitrios Maroudas**[3]

[1] Department of Physics, University of Massachusetts Amherst, Amherst, Massachusetts 01003, United States of America
[2] Department of Mechanical and Industrial Engineering, University of Massachusetts Amherst, Amherst, Massachusetts 01003, United States of America
[3] Department of Chemical Engineering, University of Massachusetts Amherst, Amherst, Massachusetts 01003, United States of America

E-mail: maroudas@ecs.umass.edu

Keywords: graphene, irradiated 2D materials, electronic structure, defect passivation, density functional theory

Abstract

We report results for the electronic structure of irradiated and irradiation-induced amorphized graphene based on first-principles density functional theory calculations, using models of irradiated graphene sheets that were initially relaxed structurally according to molecular-dynamics simulations. We find that localized states appear at the Fermi level upon irradiation damage and the corresponding local density of states increases with increasing defect density. Electronic structure calculations show that band flattening occurs due to electron localization in the vicinity of irradiation-induced defects and reduces the charge carrier mobility. This band flattening effect becomes stronger with increasing defect density due to a greater degree of carrier localization at irradiation-induced carbon dangling bonds. Passivating these dangling bonds with hydrogen atoms delocalizes the charge density, reduces the density of states at the Fermi level, and increases the band dispersion. Hydrogen passivation also has the additional effect of quenching any localized magnetic moments at dangling bonds. Our studies show that defect engineering of graphene—even at a gross level without atomic-scale precision—can be employed to tune its properties for additional electronic functionality.

1. Introduction

Graphene, a monolayer of sp^2-hybridized carbon atoms, has been studied broadly due to its exceptional electronic properties, originating from the unique behavior of the electrons (massless Dirac fermions) in the 2D honeycomb lattice, and has opened up exciting opportunities for novel nanoelectronic devices [1–5]. The electronic structure of perfect graphene can be influenced by many factors, such as the presence of impurities, defects, or dopants; hence, it can be tailored toward specific applications as reported in many studies [3, 6–15]. In particular, structural defects, which are quite common in graphene, can significantly alter its electronic structure. Different types of defects, such as point defects (i.e., single vacancies, Stone-Wales defects, etc.) and line defects (grain boundaries) are directly observed in experiments via transmission electron microscopy (TEM) and scanning tunneling microscopy (STM) [16–20]. Such defects can be formed during the graphene growth process or, alternatively, can be created in a more controlled manner, using electron or ion irradiation [16, 19, 21]. Recent studies have shown that these defects can alter the local electronic structure of graphene and/or introduce local magnetic moments [17, 18, 22–27]. Several studies have also reported that dangling bonds from under-coordinated C atoms in irradiated graphene induce localized electronic states at the Fermi level, and that these states decay in a manner that is inversely proportional to their distance from the defects [7, 23, 24, 28]. Furthermore, at a single vacancy, Jahn-Teller distortions [29] induced by reconstructions of dangling bonds are known to induce localized magnetic moments at the defect center [23–27].

While it is important to study the impact of specific defects on the electronic properties of graphene, it is also worth investigating the collective impact of diverse populations of defects that are more representative of the damage induced by electron irradiation in experiments. Toward this end, the electronic structure of electron-

irradiated samples was studied previously [6] using a density functional tight binding (DFTB) method [30]. The computer-generated irradiated graphene sheets [6] exhibited an increasing (nonvanishing) electronic density of states at the Fermi level with increasing defect density, i.e., a metallic character as a result of introducing localized states near the Fermi level [6], which are analogous to those emerging from the presence of dangling bonds due to the introduction in the graphene lattice of a low concentration of isolated single vacancies [7, 28].

In this study, using molecular-dynamics (MD) simulations followed by first-principles density functional theory (DFT) calculations, we simulate and analyze the electronic structure of irradiated and irradiation-induced amorphized graphene. It should be mentioned that the MD simulations, according to a classical bond-order potential, were performed merely as a method of initial structural relaxation in order to generate models of the irradiated structures, which have structural features consistent with experimental observations on electron-irradiated graphene sheets as reported in our earlier studies [6, 31–33]. We compare the electronic structures of hydrogen-passivated irradiated graphene configurations with those of their unpassivated counterparts and obtain a fundamental understanding of the effects of passivating irradiation-induced dangling bonds. Furthermore, we examine the magnetic behavior of these unpassivated and passivated irradiated structures based on spin-polarized DFT calculations to understand the origin of magnetic properties in these structures, and the effects of hydrogen passivation on these phenomena. Our studies show that irradiation-induced damage and chemical passivation can be used in synergy to tailor the electronic properties of graphene and, importantly, such control can be achieved via defect engineering even at a gross scale without the need for atomic-level precision.

2. Computational model and methods

In this study, to simulate irradiated graphene sheets, we used a 2×2 nm^2 (9×9) graphene supercell, which consists of 180 carbon atoms, by introducing a random distribution of vacancies, at a prescribed concentration c, followed by full structural relaxation similar to the generation of irradiated graphene configurations in our previous studies [6, 31–33]. A systematic structural relaxation of these samples based on MD simulation, with interatomic interactions described according to the AIREBO potential [34], was performed by implementing a variant of simulated annealing using a Nosé-Hoover thermostat and barostat followed by Monte Carlo (MC) relaxation based on a time-stamped force-biased MC (tfMC) algorithm [35] implemented in LAMMPS [36, 37], as introduced in our recent study [33]. These empirically relaxed structures were then further optimized using a conjugate gradient algorithm with total energy and forces on each atom computed based on first-principles density functional theory (DFT), as implemented in the Dmol^3 package in Materials Studio 8.0, in the generalized gradient approximation (GGA) with exchange and correlation functionals as parameterized by Perdew, Burke, and Ernzerhof (PBE) [38]. In this DFT implementation, the interactions between core and valence electrons were described by density functional semi-core pseudopotentials (DSPPs) [39]. Furthermore, in our DFT calculations, the wave functions were represented numerically, with a real-space orbital cutoff of 3.7Å, as expansions of Double Numerical Plus (DNP) basis sets, which include a polarization p-function on all hydrogen atoms. Monkhorst-Pack (MP) grids were employed for **k**-point sampling in reciprocal space [40]. Atomic positions were relaxed with an energy tolerance of 2×10^{-6} eV, a force tolerance of 1×10^{-3} eV/Å, and a displacement tolerance of 5×10^{-3} Å. All calculations were carried out with a 20 Å thick vacuum layer in the direction normal to the graphene sheets to avoid interactions between periodic images. The electronic band structure calculations were performed along high symmetry lines—as seen in the inset of figure 2(b1)—with **k**-point separation of 0.001 Å^{-1} and the electronic densities of states were calculated using a well-converged $7 \times 7 \times 1$ **k**-point grid. We calculated the local density of states at the Fermi energy and the spin-polarized charge densities using the CASTEP module in Materials Studio, which employs a DFT plane-wave pseudopotential method. These CASTEP calculations were performed as single-point energy calculations with a self-consistent field (SCF) tolerance of 1×10^{-6} eV following the Dmol^3 geometrical optimization. We also performed numerical tests on a few sample configurations with the plane-wave Vienna *ab initio* simulation package (VASP) [41–45] to corroborate the Dmol^3 results.

Representative fully relaxed configurations of our model irradiated graphene structures are shown in figure 1, over a range of inserted vacancy concentration, c, up to 20%. In agreement with our previous empirical-potential studies on larger irradiated graphene supercells (i.e., 6×6 nm^2 or larger) [6, 31–33], the smaller supercells employed here also exhibit vacancy coalescence and reconstruction-induced wrinkling and crumpling of the graphene sheets while maintaining their coherent 2D structure. On applying the more accurate DFT optimization step to the relaxed empirical potential structures, we observe a few additional ring reconstructions at defects mediated by energetically favored Jahn-Teller distortions [21, 46].

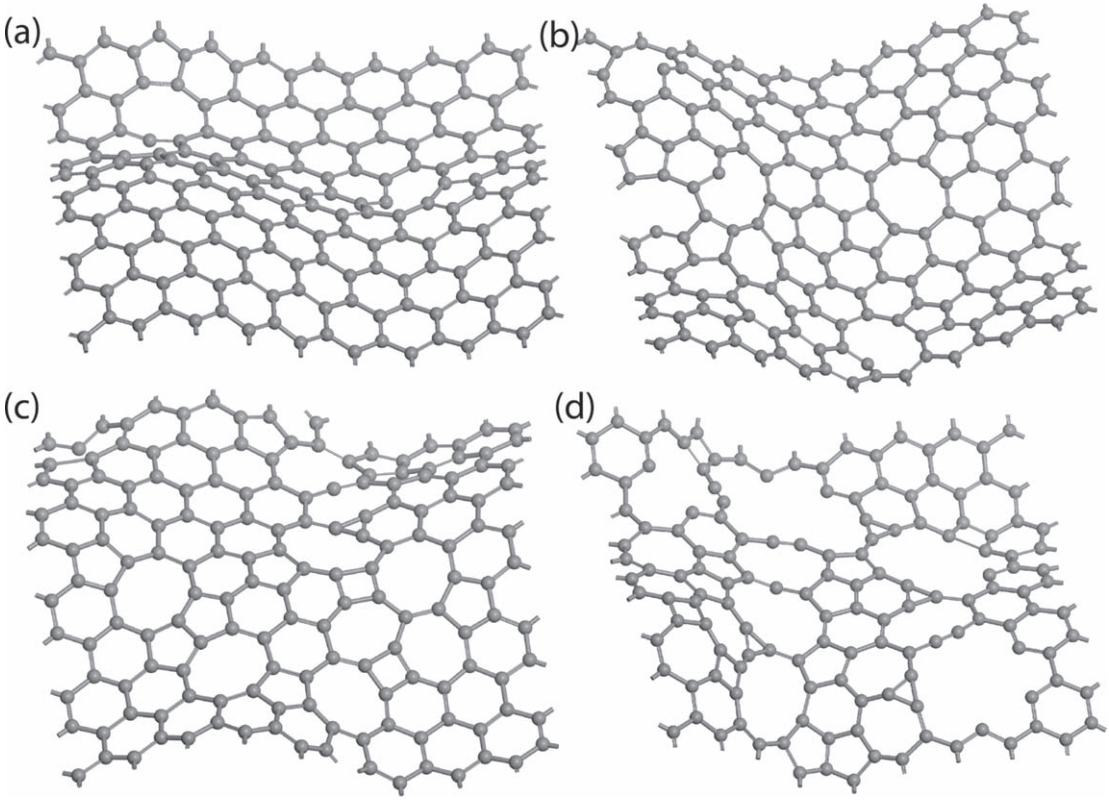

Figure 1. Representative structurally relaxed and optimized (according to DFT computations) atomic configurations of irradiated graphene sheets with inserted vacancy concentration, *c*, of (a) 2%, (b) 4%, (c) 10%, and (d) 20%.

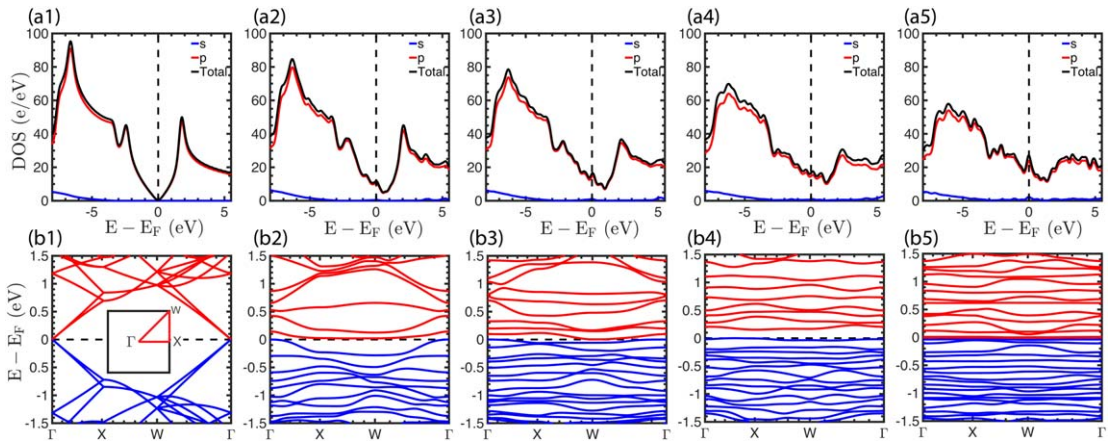

Figure 2. (a) Orbital-resolved (partial) and total electronic densities of states of (a1) perfect and (a2–a5) irradiated graphene sheets with an inserted vacancy concentration, *c*, of (a2) 2%, (a3) 4%, (a4) 10%, and (a5) 20%. Partial electronic densities of states corresponding to *s* and *p* orbitals are represented by blue and red lines, respectively, while the total electronic density of states is represented by the black line. In all cases (a1–a5), the Fermi level is marked by the dashed vertical line. (b) Electronic band structures of (b1) perfect and (b2–b5) irradiated graphene sheets with a *c* of (b2) 2%, (b3) 4%, (b4) 10%, and (b5) 20%. In all cases (b1–b5), the horizontal black dashed line denotes the Fermi energy (E_F), while red and blue lines represent conduction and valence bands, respectively. The inset in (b1) shows the first Brillouin zone and the high-symmetry **k** points.

3. Electronic structure and effects of hydrogen passivation

Figures 2(a2)–(a5) show the orbital-resolved (partial) density of states for the irradiated structures with an inserted vacancy concentration, *c*, of 2%, 4%, 10% and 20%, respectively; these densities of states are statistically averaged over three independently generated configurations at each vacancy concentration. The density of states (DOS) of these irradiated structures demonstrates clearly the emergence of localized states at the Fermi level in contrast to the vanishing states in perfect single-layer graphene, which is shown in figure 2(a1). These states at

the Fermi level increase in magnitude and bandwidth with increasing vacancy concentration, as seen in earlier DFTB calculations [6] and consistent with other theoretical investigations [7, 28]; these states appear mainly due to the presence of dangling bonds from under-coordinated carbon atoms in the defective (damaged) irradiated structure. The orbital-resolved density of states reveals that the new states at the Fermi level originate clearly from the carbon *p* orbitals with only a minor contribution from *s* orbitals, and increase with increasing defect density. We also note the progressive softening of the characteristic van Hove singularities of graphene with increasing defect density.

The electronic band structures, E(*k*) dispersion relations, of our irradiated graphene sheets corresponding to the configurations of figure 1 are shown in figures 2(b2)–(b5). The band structure of perfect graphene exhibits the characteristic linear band dispersion and formation of Dirac cones at the Γ point, as shown in figure 2(b1), where the K point in the graphene unit cell has been mapped onto the Γ point of the chosen supercell. This linear dispersion of the bands mimics the behavior of quasi-particles known as massless Dirac fermions which gives pristine, structurally perfect graphene its extremely high carrier mobility [2, 4]. On the contrary, in the irradiated structures, the Dirac cones disappear from the band structure and flat or nearly flat bands appear instead. It has been reported that the splitting of the dangling-bond states, due to the crystal field and Jahn-Teller distortions, breaks trigonal symmetry, thereby removing the degeneracy and generating these flat bands [23, 47]. Furthermore, these flat bands result in the reduction of the mobility of charge carriers, by increasing their effective mass, which is inversely proportional to the band curvature ($m^* = \hbar^2\left(\frac{d^2E_k}{dk^2}\right)^{-1}$, where *k* is the wave number and E_k is the energy corresponding to the wave number *k*), and cause charge carriers to be highly localized in the defective regions [48, 49]. Moreover, it has been shown that both strain and isolated vacancies can reduce the linear dispersion, introduce Fermi level shifting, manifest metallic behavior by band crossing, and also introduce very narrow direct and indirect band gaps [49, 50]. As seen in figure 2(b), in our irradiated structures, which are characterized by larger defects and higher local strain, many more flat bands are introduced in the band structures, which correspond to non-interacting orbitals. This band flattening effect becomes stronger with increasing vacancy concentration, *c*, which emphasizes that the electrons are more localized in highly defective irradiated structures. Furthermore, we have identified the opening of narrow band gaps (on the order of 10 meV), which are independent of the inserted vacancy concentration but specific to each damaged structure.

The origin of the localized states seen in the DOS and band-structure plots can be probed by analyzing the real-space distribution of these states. Figure 3(a) displays the charge density of conduction electrons near the Fermi level, from which it is clear that these localized states in the DOS arise from electrons at carbon dangling bonds. Interestingly, there is little to no contribution to these localized states from monoatomic C chains in the highly damaged regions of the irradiated structures, which is likely due to these C atoms becoming *sp*–hybridized. On average, more energetically favored ring reconstructions also do not induce local states; however, some reconstructions do induce new states due to local stresses arising from such bond rearrangements, which can be seen especially in the more damaged structures of figures 3(a3)–(a4). These electron density distributions also serve to highlight the reactive dangling bonds within the defective graphene sheets, thereby providing a template for systematic passivation of these structures [51], which we consider next.

Guided by the electron density distributions of the frontier orbitals, highly under-coordinated carbon atoms were chemically passivated with hydrogen by allowing two hydrogen atoms to bond to a selected carbon atom. The passivated structures were then relaxed with DFT-based structural optimization, and representative relaxed configurations are shown in figure 3(b). Subsequently, electronic structure calculations similar to those on the unpassivated irradiated structures were performed to assess the effects of hydrogen passivation on the electronic structure of the irradiated graphene sheets. By inspecting the electron density distributions of the hydrogen-passivated irradiated structures of figure 3(c) for the inserted vacancy concentrations of 2%, 4%, 10%, and 20%, it is evident that there is no more contribution to the local electron density at the Fermi level from the passivated C atoms. New localized states now appear in the immediate vicinity of the passivated C atoms and can act as possible adsorption sites for further passivation of these irradiated sheets. Furthermore, by comparing the isosurface values for each case of figure 3(c) with those of the corresponding unpassivated structures of figure 3(a), we see that these newly-emergent states are more diffuse than the original dangling-bond states and can promote carrier hopping through the structure.

Figure 4(a) shows the orbital-resolved DOS for these hydrogenated structures as a function of inserted vacancy concentration, *c*. The defect-induced local density of states at the Fermi level decreases as a result of the passivation and the contribution from the *s* orbitals, at the Fermi level, is completely diminished. Figure 4(b) shows the corresponding band structures for these passivated structures and, in comparison with the unpassivated cases (figure 2(b)), we note that some dispersion (increased curvature) is now restored to the flat bands. Thus, hydrogen passivation of the dangling bonds reduces carrier masses by delocalizing the dangling-bond states as discussed previously in the analysis of the electron density distributions. Furthermore, this

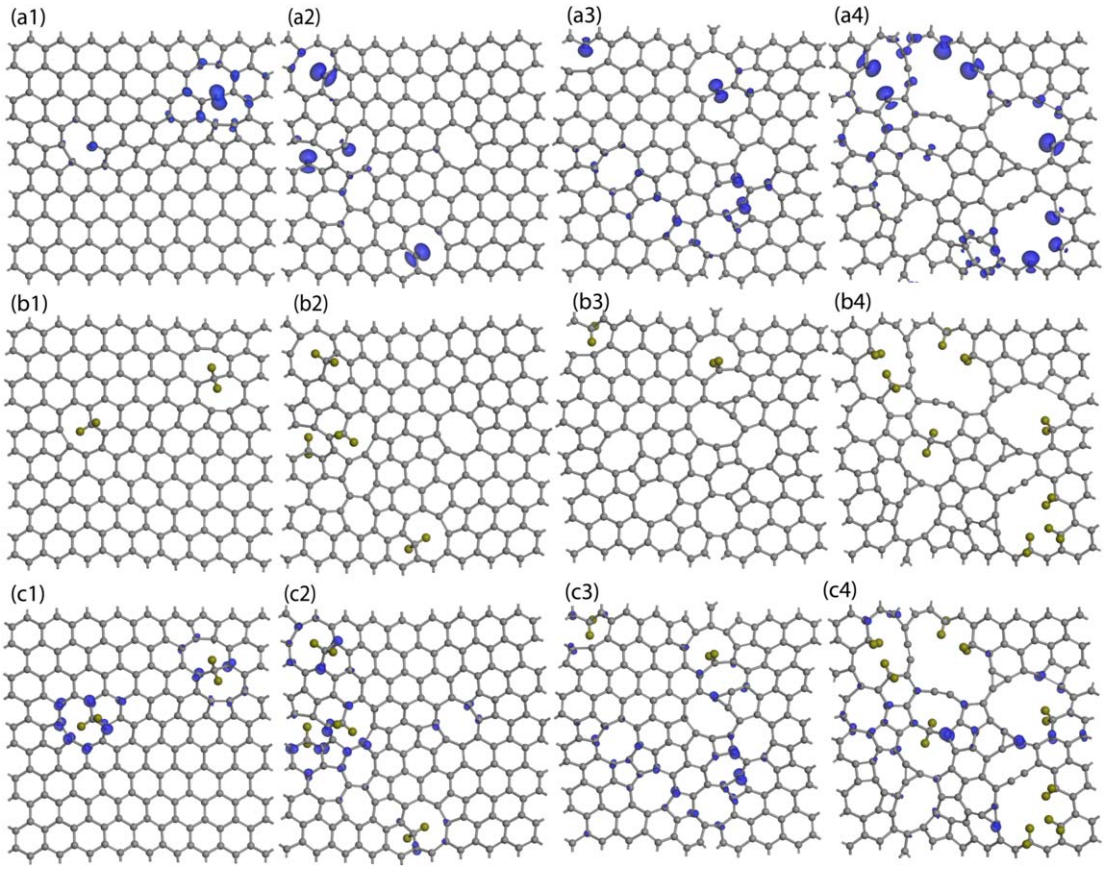

Figure 3. (a) Isosurfaces of electronic charge density at an applied bias of 1 V above the Fermi level, with isovalues in the range of 0.05–0.09 e/Å^3 in representative atomic configurations of irradiated graphene sheets with inserted vacancy concentrations, *c*, of (a1) 2%, (a2) 4%, (a3) 10%, and (a4) 20%. In each case, different isovalues have been used to properly highlight the contributions from the newly induced electronic states in the vicinity of the Fermi level. (b) Representative structurally relaxed and optimized (according to DFT computations) atomic configurations of hydrogen-passivated graphene sheets with *c* levels of (b1) 2%, (b2) 4%, (b3) 10%, and (b4) 20%. (c) Isosurfaces of electronic charge density at an applied bias of 1 V above the Fermi level, with isovalues in the range of 0.05–0.09 e/Å^3 in representative atomic configurations of hydrogen-passivated irradiated graphene sheets; the maps of (c1), (c2), (c3), and (c4) correspond to the atomic configurations of (b1), (b2), (b3), and (b4). In each case (c1–c4), the same isovalues with those of the corresponding unpassivated irradiated structures in (a1–a4) have been used to emphasize the hydrogen passivation effect on the local density of states. In all cases, silver and olive green spheres represent C and H atoms, respectively.

increase in the band dispersion can result in different responses in the materials' metallic behavior and opening of narrow band gaps that can be direct or indirect, as can be seen in figure 4(b), which may be characteristic of a specific irradiated configuration; however, this band dispersion increase does not impact the overall trend in the electronic character of the material related to the level of disorder in the irradiated structures. Moreover, the decrease in band flattening is most noticeable in structures with more dispersed sites possessing dangling bonds, such as that of figure 1(d), as observed clearly in figure 2(b5). Such structural features cause a large number of flat bands to appear near the Fermi level; nevertheless, the passivation of the dangling bonds removes a substantial amount of those flat bands and increases the dispersion, figure 4(b4), hence delocalizing carriers, as can be seen in figure 3(c4).

4. Local spin polarization and effects of hydrogen passivation

The splitting of the dangling-bond states due to both the crystal field and the Jahn-Teller distortion from the reconstruction of vacancies is known to introduce a net magnetic moment at under-coordinated carbon atoms [22, 25, 27, 47, 52]. Figure 5 displays spin-density isosurfaces for the unpassivated and hydrogen-passivated defective graphene structures at various levels of defect concentration. In all of the unpassivated configurations shown in figure 5(a), we clearly see that the localized spin states appear at the dangling-bond sites. For lower vacancy concentrations (i.e., 2% and 4%), we observe the well-known 5–9 reconstructions of graphene monovacancies with a magnetic moment localized at the under-coordinated carbon atom [22, 25, 27, 47]. However, the more damaged structures, characterized by much stronger distortions and formation of larger voids, can also exhibit local spin-polarized states as seen in figure 5(a4). While these heavily defective lattices

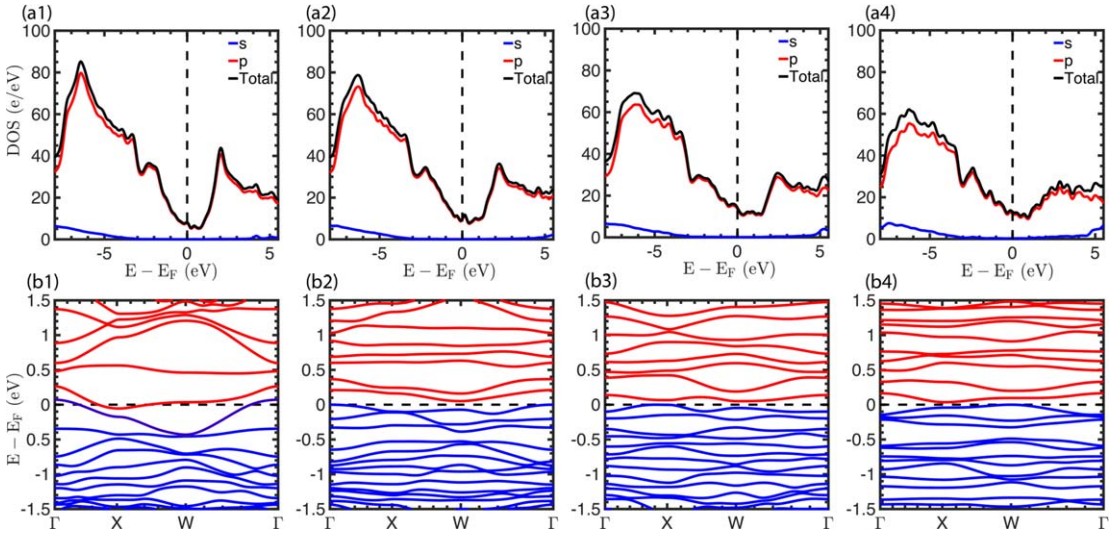

Figure 4. (a) Orbital-resolved (partial) and total electronic densities of states of hydrogen-passivated irradiated graphene sheets with an inserted vacancy concentration, *c*, of (a1) 2%, (a2) 4%, (a3) 10%, and (a4) 20%. Partial electronic densities of states corresponding to *s* and *p* orbitals are represented by blue and red lines, respectively, while the total electronic density of states is represented by the black line. In all cases (a1–a4), the Fermi level is marked by the dashed vertical line. (b) Electronic band structures of hydrogen-passivated irradiated graphene sheets with a *c* of (b1) 2%, (b2) 4%, (b3) 10%, and (b4) 20%. In all cases (b1–b4), the horizontal black dashed line denotes the Fermi energy (E_F), while red and blue lines represent conduction and valence bands, respectively.

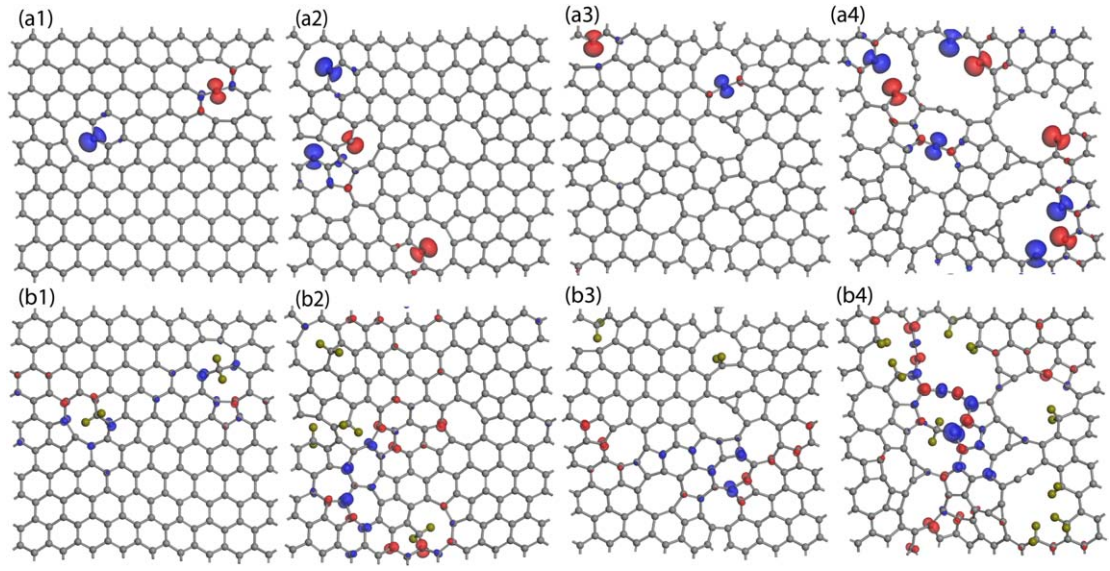

Figure 5. (a) Contour maps of electron spin density, at isovalues of ± 0.06 e/Å^3, where red and blue denote positive and negative spin density, respectively, in representative atomic configurations of irradiated graphene sheets with inserted vacancy concentrations, *c*, of (a1) 2%, (a2) 4%, (a3) 10%, and (a4) 20%. (b) The analogous contour maps of electron spin density, at isovalues of ± 0.003 e/Å^3, with the same color coding as in (a) in representative atomic configurations of hydrogen-passivated irradiated graphene sheets with *c* levels of (b1) 2%, (b2) 4%, (b3) 10%, and (b4) 20%. In all cases, silver and olive green spheres are used to denote C and H atoms, respectively.

might not lend themselves to immediate application of Lieb's theorem for bipartite lattices [53, 54], we nevertheless find that an odd number of dangling bonds results in a net magnetic moment in these structures. Hydrogenation of dangling bonds quenches the localized magnetic moments, as seen by comparing the electron spin density distributions of the unpassivated structures (figure 5(a)) to those of the passivated structures (figure 5(b)). The more diffusely distributed magnetic moments in the vicinity of the hydrogenated C atoms are over an order of magnitude smaller than the original moments at the dangling-bond sites. Thus, hydrogen passivation of the irradiated graphene sheets plays a dual role of quenching local magnetic moments while also restoring a degree of mobility to charge carriers.

5. Summary and conclusions

In summary, we have performed systematic studies of the electronic structure of irradiated graphene sheets and the effects of passivation of irradiation-induced defects on the electronic structure. We have identified several interesting characteristics of the electronic structure of irradiated graphene based on first-principles DFT calculations. We have found that localized states appear at the Fermi level upon irradiation and the corresponding local density of states increases with increasing defect density. Furthermore, band-structure calculations have shown that band flattening occurs due to electron localization in the vicinity of irradiation-induced defects and reduces the charge carrier mobility. This band flattening effect becomes stronger with increasing defect density, inducing a greater number of flat bands near the Fermi level. Local density of states plots provide clear evidence of such carrier localization near dangling bonds. Passivating carbon dangling bonds near the Fermi level with hydrogen atoms leads to delocalization of the charge density, hence increasing the carrier mobility, which also is seen in the reduced density of states observed at the Fermi level and the increased band dispersion with increasing defect density. An additional effect of hydrogen passivation is to quench the localized magnetic moments at carbon dangling bonds. The fundamental understanding of the electronic structure of unpassivated and hydrogen-passivated irradiated graphene sheets obtained by our studies now sets the stage for designing electronic nanomaterials for specific applications using irradiated graphene and passivated irradiated graphene as a well-understood template.

Acknowledgments

This work was supported by the Army Research Laboratory under Grant No. W911NF-11-2-0014.

ORCID iDs

Asanka Weerasinghe https://orcid.org/0000-0001-7749-6823
Dimitrios Maroudas https://orcid.org/0000-0001-9297-8839

References

[1] Novoselov K S, Geim A K, Morozov S V, Jiang D, Zhang Y, Dubonos S V, Grigorieva I V and Firsov A A 2004 Electric field effect in atomically thin carbon films *Science* **306** 666–9
[2] Geim A K and Novoselov K S 2007 The rise of graphene *Nat. Mater.* **6** 183–91
[3] Castro Neto A H, Guinea F, Peres N M R, Novoselov K S and Geim A K 2009 The electronic properties of graphene *Rev. Mod. Phys.* **81** 109–62
[4] Geim A K 2009 Graphene: status and prospects *Science* **324** 1530–4
[5] Abergel D, Apalkov V, Berashevich J, Ziegler K and Chakraborty T 2010 Properties of graphene: a theoretical perspective *Adv. Phys.* **59** 261–482
[6] Carpenter C, Ramasubramaniam A and Maroudas D 2012 Analysis of vacancy-induced amorphization of single-layer graphene *Appl. Phys. Lett.* **100** 203105
[7] Pereira V M, Guinea F, Lopes dos Santos J M B, Peres N M R and Castro Neto A H 2006 Disorder induced localized states in graphene *Phys. Rev. Lett.* **96** 036801
[8] Yazyev O V and Louie S G 2010 Electronic transport in polycrystalline graphene *Nat. Mater.* **9** 806
[9] Pedersen T G, Flindt C, Pedersen J, Mortensen N A, Jauho A P and Pedersen K 2008 Graphene antidot lattices: Designed defects and spin qubits *Phys. Rev. Lett.* **100** 136804
[10] Qin X, Meng Q and Zhao W 2011 Effects of Stone-Wales defect upon adsorption of formaldehyde on graphene sheet with or without al dopant: a first principle study *Surf. Sci.* **605** 930
[11] Banhart F, Kotakoski J and Krasheninnikov A V 2011 Structural defects in graphene *ACS Nano* **5** 26
[12] Pereira V M, Castro Neto A H and Peres N M R 2009 Tight-binding approach to uniaxial strain in graphene *Phys. Rev.* B **80** 045401
[13] Adam S, Hwang E, Rossi E and Das Sarma S 2009 Theory of charged impurity scattering in two-dimensional graphene *Solid State Commun.* **149** 1072–9
[14] Zhang L, Xu Q, Niu J and Xia Z 2015 Role of lattice defects in catalytic activities of graphene clusters for fuel cells *Phys. Chem. Chem. Phys.* **17** 16733–43
[15] Gómez-Arias W A and Naumis G G 2016 Analytical calculation of electron group velocity surfaces in uniform strained graphene *Int. J. Mod. Phys.* B **30** 1550263
[16] Kotakoski J, Krasheninnikov A V, Kaiser U and Meyer J C 2011 From point defects in graphene to two-dimensional amorphous carbon *Phys. Rev. Lett.* **106** 105505
[17] Ugeda M M, Brihuega I, Guinea F and Gómez-Rodríguez J M 2010 Missing atom as a source of carbon magnetism *Phys. Rev. Lett.* **104** 096804
[18] Kondo T, Honma Y, Oh J, Machida T and Nakamura J 2010 Edge states propagating from a defect of graphite: Scanning tunneling spectroscopy measurements *Phys. Rev.* B **82** 153414
[19] Urban K W *et al* 2008 Studying atomic structures by aberration-corrected transmission electron microscopy *Science* **321** 506–10
[20] Tapasztó L, Nemes-Incze P, Dobrik G, Jae Yoo K, Hwang C and Biró L P 2012 Mapping the electronic properties of individual graphene grain boundaries *Appl. Phys. Lett.* **100** 053114

[21] Lehtinen O, Kotakoski J, Krasheninnikov A V, Tolvanen A, Nordlund K and Keinonen J 2010 Effects of ion bombardment on a two-dimensional target: Atomistic simulations of graphene irradiation *Phys. Rev.* B **81** 153401
[22] Lehtinen P O, Foster A S, Ma Y, Krasheninnikov A V and Nieminen R M 2004 Irradiation-induced magnetism in graphite: a density functional study *Phys. Rev. Lett.* **93** 187202
[23] Nanda B R K, Sherafati M, Popović Z S and Satpathy S 2012 Electronic structure of the substitutional vacancy in graphene: density-functional and Green's function studies *New J. Phys.* **14** 083004
[24] Faccio R, Fernández-Werner L, Pardo H, Goyenola C, Ventura O N and Mombrú Á W 2010 Electronic and structural distortions in graphene induced by carbon vacancies and boron doping *J. Phys. Chem.* C **114** 18961–71
[25] Yazyev O V and Helm L 2007 Defect-induced magnetism in graphene *Phys. Rev.* B **75** 125408
[26] Popović Z S, Nanda B R K and Satpathy S 2012 Nuclear tunneling and dynamical Jahn-Teller effect in graphene with vacancy *Phys. Rev.* B **86** 085458
[27] Chen J J, Wu H C, Yu D P and Liao Z M 2014 Magnetic moments in graphene with vacancies *Nanoscale* **6** 8814
[28] Pereira V M, Lopes dos Santos J M B and Castro Neto A H 2008 Modeling disorder in graphene *Phys. Rev.* B **77** 115109
[29] Jahn H A and Teller E 1937 Stability of polyatomic molecules in degenerate electronic states - I—orbital degeneracy *Proc. R. Soc.* A **161** 220–35
[30] Aradi B, Hourahine B and Frauenheim T 2007 DFTB+, a sparse matrix-based implementation of the DFTB method *J. Phys. Chem.* A **111** 5678
[31] Carpenter C, Maroudas D and Ramasubramaniam A 2013 Mechanical properties of irradiated single-layer graphene *Appl. Phys. Lett.* **103** 013102
[32] Weerasinghe A, Muniz A R, Ramasubramaniam A and Maroudas D 2016 Mechanical properties of hydrogenated electron-irradiated graphene *J. Appl. Phys.* **120** 124301
[33] Weerasinghe A, Ramasubramaniam A and Maroudas D 2017 Thermal conductivity of electron-irradiated graphene *Appl. Phys. Lett.* **111** 163101
[34] Stuart S J, Tutein A B and Harrison J A 2000 A reactive potential for hydrocarbons with intermolecular interactions *J. Chem. Phys.* **112** 6472
[35] Mees M J, Pourtois G, Neyts E C, Thijsse B J and Stesmans A 2012 Uniform-acceptance force-bias Monte Carlo method with time scale to study solid-state diffusion *Phys. Rev.* B **85** 134301
[36] Neyts E C and Bogaerts A 2012 Combining molecular dynamics with Monte Carlo simulations: implementations and applications *Theor. Chem. Acc.* **132** 1320
[37] Bal K M and Neyts E C 2014 On the time scale associated with Monte Carlo simulations *J. Chem. Phys.* **141** 204104
[38] Perdew J P, Burke K and Ernzerhof M 1996 Generalized gradient approximation made simple *Phys. Rev. Lett.* **77** 3865–8
[39] Delley B 2002 Hardness conserving semilocal pseudopotentials *Phys. Rev.* B **66** 155125
[40] Monkhorst H J and Pack J D 1976 Special points for Brillouin-zone integrations *Phys. Rev.* B **13** 5188–92
[41] Kresse G and Hafner J 1993 *Ab initio* molecular dynamics for liquid metals *Phys. Rev.* B **47** 558–61
[42] Kresse G and Furthmüller J 1996 Efficiency of *ab-initio* total energy calculations for metals and semiconductors using a plane-wave basis set *Comput. Mater. Sci.* **6** 15–50
[43] Kresse G and Furthmüller J 1996 Efficient iterative schemes for *ab initio* total-energy calculations using a plane-wave basis set *Phys. Rev.* B **54** 11169–86
[44] Kresse G and Joubert D 1999 From ultrasoft pseudopotentials to the projector augmented-wave method *Phys. Rev.* B **59** 1758–75
[45] Blöchl P E 1994 Projector augmented-wave method *Phys. Rev.* B **50** 17953–79
[46] El-Barbary A A, Telling R H, Ewels C P, Heggie M I and Briddon P R 2003 Structure and energetics of the vacancy in graphite *Phys. Rev.* B **68** 144107
[47] Paz W S, Scopel W L and Freitas J C 2013 On the connection between structural distortion and magnetism in graphene with a single vacancy *Solid State Commun.* **175-176** 71–5
[48] Zhang W, Lu W C, Zhang H X, Ho K and Wang C 2016 Lattice distortion and electron charge redistribution induced by defects in graphene *Carbon* **110** 330–5
[49] Surya V J, Iyakutti K, Mizuseki H and Kawazoe Y 2012 Tuning electronic structure of graphene: a first-principles study *IEEE Trans. Nanotechnol.* **11** 534–41
[50] Kim D H, Kim M S and Kim H D 2015 Geometrical and electronic structures of graphene under different vacancy density and configuration *Appl. Surf. Sci.* **359** 55–60
[51] Hou Z, Wang X, Ikeda T, Terakura K, Oshima M, Kakimoto M and Miyata S 2012 Interplay between nitrogen dopants and native point defects in graphene *Phys. Rev.* B **85** 165439
[52] Dai X Q, Zhao J H, Xie M H, Tang Y N, Li Y H and Zhao B 2011 First-principle study of magnetism induced by vacancies in graphene *Eur. Phys. J.* B **80** 343–9
[53] Lieb E and Mattis D 1962 Ordering energy levels of interacting spin systems *J. Math. Phys.* **3** 749–51
[54] Lieb E H 1989 Two theorems on the Hubbard model *Phys. Rev. Lett.* **62** 1201–4